Estuarine, Coastal and Shelf Science 223 (2019) 61–73

Contents lists available at ScienceDirect

Estuarine, Coastal and Shelf Science

journal homepage: www.elsevier.com/locate/ecss

Factors controlling saltwater intrusion across multi-time scales in estuaries, Chester River, Chesapeake Bay

Richard Tian*

University of Maryland Center for Environmental Science, 410 Severn Avenue, Annapolis, 21403, MD, USA

ARTICLE INFO

Keywords:
Chesapeake Bay
Modeling
Saltwater intrusion
Interannual variability

ABSTRACT

The relative dominance of controlling factors in saltwater intrusion depends on the time scale in which the variability in characterized. Long-term time series data of salinity and temperature has been collected in the Chester River, Chesapeake Bay, showing considerable variabilities of saltwater intrusion with time scales from days to years. In this study, the Finite-Volume Community Ocean Model (FVCOM) was applied to the data over a decadal time scale from 2002 to 2011 to identify the drivers and their relative importance in controlling the variability of saltwater intrusion with different time scale ranging from events of a few days, through seasonal to interannual variations. FVCOM successfully reproduced the observed variations in saltwater intrusion over the entire simulation period, and thus completed time series data from monthly samples to daily and even at a higher temporal resolution for statistical analysis. The results shows that river discharge is the primary factor controlling the saltwater intrusion variability on interannual time scales, but sea surface level is more dominating on seasonal variations, while wind has more important influence on short-time scales during weather events, mostly through modulation of sea surface level on regional scales rather than local wind strain and Ekman transport. Tide has limited influence due to short tidal excursion and amplitude in the Chester Estuary. The estuarine geometry has a significant influence on the two-layer estuarine circulation and saltwater intrusion in the Chester Estuary. The upper estuary is the shallow narrow channel where two-layer estuarine circulation is limited, the meanders in the mid-estuary also restrict the development of the two-layer circulation due to helical circulation, while the lower estuary has stronger stratification and two-layer circulation as compared to the upper and mid-estuary.

1. Introduction

Saltwater intrusion in one of the fundamental aspect of estuaries and its variations have profound impacts of freshwater resources and the livelihood of the surrounding population and development. Freshwater discharge, sea surface level, tide, wind, waves, storm surge, estuary shape and topography all influence the extent and variation in saltwater intrusion (Savenije, 1993; Zhang and Deng, 2010). Monismith et al. (2002) scaled the buoyancy-driven circulation to the 1/3 power of runoff and the saltwater intrusion to the negative 1/3 power of runoff. Festa and Hansen (1976) found that saltwater intrusion extent varies with the estuary Rayleigh number which is proportional to the cubic bathymetry. At given bathymetry and shape of an estuary, the functionality of saltwater intrusion depends on the type of estuaries and the balance between freshwater discharge and salt water propagation from tide and sea level surge. In well mixed estuaries (Richardson number $Ri < 0.08$), there is no distinct stratification and saltwater moves forth and back with tide and freshwater discharge and can be flushed out of the estuary by extreme high runoff events (MacCready et al., 2002; Lerczak et al., 2008; Kuijper and Van Rijn, 2011). In partially mixed ($0.08 < Ri < 0.8$) and saltwater wedge estuaries, the water circulation is dominated by the two-layer gravitation circulation (also called estuarine circulation, reaction current, induction current, undercurrent, compensatory bottom current and baroclinic flow; Beardsley and Boicourt, 1981), with freshwater mostly flow out in the surface layer whereas saltwater propagates upstream in the bottom layer. Saltwater intrusion depends on freshwater discharge, sea surface level at the mouth, tide, stratification, density gradient and vertical mixing strength. Ralston et al. (2008) found that increased freshwater discharge lead to decreasing in vertical mixing and increasing in Richardson number and gravitational circulation. Asymmetric tidal mixing, lateral circulation and convective overturning all contribute to the two-layer residual circulation. Stronger vertical mixing during flood tide in shallow regions bring salt water from the bottom to the surface

* UMCES/CBPO, 410 Severn Avenue, Annapolis, 21403, MD, USA.
E-mail address: rtian@umces.edu.

https://doi.org/10.1016/j.ecss.2019.04.041
Received 11 December 2018; Received in revised form 22 April 2019; Accepted 23 April 2019
Available online 26 April 2019

layer where it flows out during ebb tide (Simpson et al., 1990, 2005; Scully and Friedrichs, 2007). Divergence is created during flood tide and convergence during ebb tide at the bottom main stem due to baroclinic pressure and topography, which enhance the two-layer estuarine circulation (Nunes and Simpson, 1985; Burchard and Schuttelaars, 2012). In wide estuaries like the Chesapeake Bay, the divergence (convergence) zone shift to the right-hand side bank (looking upstream) and creating cross-estuary lateral circulation and tilting isopycnocline (Huijts et al., 2009; Basdurak and Valle-Levinson, 2013). Convective overturning due to tidal straining and baroclinic instability at the end of the flood increases water exchange between the two layers and thus enhances the two-layer residual circulation (Simpson et al., 1990, 2005; Nepf and Geyer, 1996; Prandle, 2004). The estuarine geometry and convergency can alter the dependency of the gravitational circulation and saltwater intrusion on river discharge (Savenije, 1993; Ralston et al., 2008; Gay and O'Donnell, 2009). Channel curvature and meandering can alter both lateral and along channel circulation through centrifugal acceleration and helical lateral flow under adequate curvature Rossby number (Lacy and Monismith, 2001; Chant, 2002; Basdurak and Valle-Levinson, 2013; Wells and Cossu, 2013). In large estuaries, cross-sectional density gradient and mixing also play a role in determining saltwater intrusion extent and intensity. In fiord estuaries, tide mostly determine the extent of saltwater propagation whereas low flow has limited influence.

Saltwater intrusion studies in Chesapeake Bay and its tributaries started with the pioneer work of Pritchard in the 1950s in the James River based on which the two-layer estuarine circulation were established (Pritchard, 1952, 1954; 1956; Hansen and Rattray, 1965). Over the years, a number of studies have been carried out, in the main stem of the Bay (Wang, 1979a; Xu et al., 2012) and its western tributaries like the Potomac River Estuary (Elliott, 1978; Wang and Elliott, 1978), and the York River Estuary (Friedrichs, 2009). Based on field measurement, Wang (1979a) argued that there are two modes that wind influences saltwater intrusion in Chesapeake Bay, one through local wind strain, and the other through Eckman transport on the continental shelf. Elliott (1978) also found the two-mode response of saltwater intrusion to wind forcing in the Potomac Estuary. In the York Estuary, however, Friedrichs (2009) reported that tide has a major influence on salinity distribution on fortnightly and even seasonal time scales. Using a hydrodynamic model, Xu et al. (2012) found that freshwater discharge is the primary factor controlling saltwater intrusion in Chesapeake Bay. However, few, if any, studies have been reported in the Chester Estuary on the eastern-shore. The Chester River is a major tributary in the Chesapeake Bay located on the eastern shore of the upper bay (Fig. 1). Its drainage area is about 950 km^2, mainly through rural area and the long-term average discharge is about 20 $m^3 s^{-1}$. Agricultural irrigation and freshwater withdrawal rely on the river and saltwater intrusion is a big concern for the population is the surrounding area. High salinity also affects local floral and faunal habitats. This paper presents a study of saltwater intrusion in the Chester River Estuary based on field observation and 3D hydrodynamic model simulations. Within the framework of the Chesapeake Bay Program, long-term monitoring time series data of salinity and temperature have been collected in the Chester Estuary, which shows large variations in saltwater intrusion. However, the samples were mostly collected at a monthly frequency, which does not cover variations in short times scales. Also, the sampling frequency differs from that of controlling factors such as river discharge, wind and sea surface level, making causality statistical analysis difficult. The three-dimensional Finite-Volume Community Model (FVCOM) was used to reproduce the observation over a decadal time scale. Once calibrated, the model provided data at various time frequencies for statistical analysis. The model application in this study is data-driven in a realistic setting, differing from model sensitivity analysis in which model response to a change in a forcing file is looked at. The Chester Estuary is also characterized with several menders and high convergency, providing an ideal configuration for comprehensive analysis of the controlling factors of saltwater intrusion across a wide range of time scales. A significant number of studies have been conducted to identify the dominant factor in controlling saltwater intrusion in estuaries, but few look at cross-time scales. Our hypothesis is that the relative dominance of controlling factors in determining saltwater intrusion is time-scale dependent. Some factors may be more dominating in short-term events, whereas other are more prevailing in long-term variations. Generalized additive model (GAM) was performed on simulated results and the forcing data to discern long-term trend, seasonal and interannual variability, followed by principal component analysis (PCA) to identify causality between the forcing data and saltwater intrusion at different time scales. The paper is organized as the following: The “Method” section describes the model platform, the forcing and observation data, and statistical analysis. The “Result” section presents comparison between simulation and data for temperature and salinity, and model predicted extent of saltwater intrusion. The “Discussion” section presents the causality statistical analysis between saltwater intrusion and forcing variables.

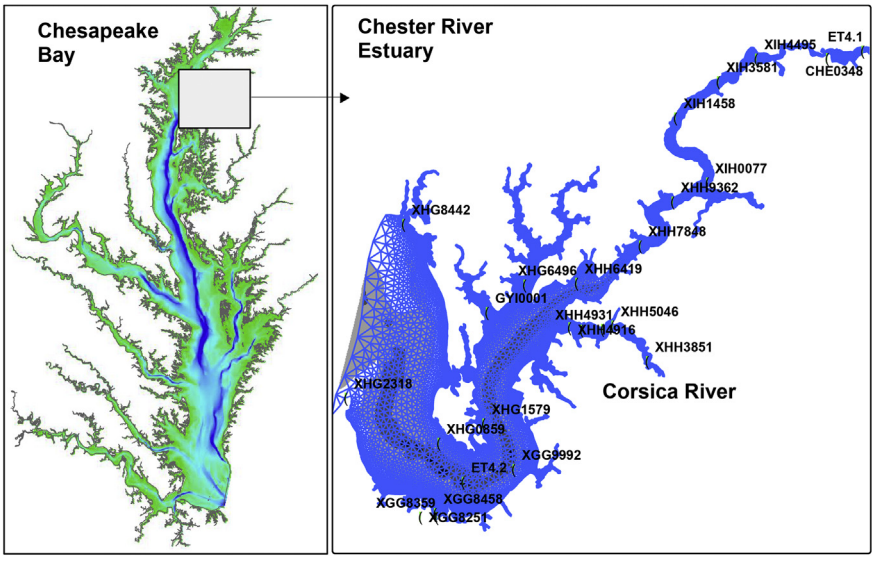

Fig. 1. Geographic location, grids, bathymetry and observation stations in the simulation domain. The left panel is Chesapeake Bay located in the states of Maryland and Virginia and Washington D.C. on the eastern shore of the U.S., and the right panel is the Chester River Estuary. Dark background indicates deep area up to 50 m in Chesapeake Bay and 18 m in the Chester River Estuary.

2. Method

2.1. Physical model

The Finite–Volume Community Ocean Model (FVCOM) was used to simulate the hydrodynamics and water properties (temperature and salinity) in this study. FVCOM is a 3D primitive equation model with unstructured-grid, general terrain-following coordinate and wet/dry treatment for the intertidal zone (Chen et al., 2003). The non-overlapping unstructured triangular grid in the horizontal has the advantage of resolving the complex coastal geometry in the Chester Estuary. In this study, a terrain-following sigma coordinate was used in the vertical, with 10 uniform layers with equal thickness. Vertical turbulent diffusivity was computed with the 2.5 level Mellor-Yamada turbulence model (Mellor and Yamada, 1982), but other option from the General Ocean Turbulence Model (GOTM) libraries are available for selection (Burchard and Bolding, 2001; Tian and Chen, 2006). Horizontal diffusivity was computed as a function of the grid cell size and current velocity based on the Smagorinsky eddy parameterization method (Smagorinsky, 1963; Chen et al., 2003).

The simulation domain extends from the fall line to the Chester River Mouth in Chesapeake Bay (Fig. 1). Grid resolution is about 1 km at the river mouth to 100 m near the coastline, with 13824 cells and 8351 nodes in total. The simulation time step is set at 2 s. The wet-dry simulation was activated during the simulation and the minimum water depth was set at 10 cm below which computation cells were treated as dry, i.e. the vertical resolution reached to 1 cm in the coastal region, limiting thus the time step. The model was first spun up for 5 years using the same forcing of 2002 and the initial condition was based on the EPA regulatory model CH3D simulation of the whole Chesapeake Bay (see the following section). Following the spinning up, the model was continuously run from 2002 to 2011.

2.2. Forcing data

FVCOM computes the net heat flux based on the bulk parameterization of air-sea exchange (Fairall et al., 1996), which requires data of long-wave and short-wave radiation, relative humidity, air temperature, pressure and wind speed. Both wind speed and direction are required for surface momentum forcing and precipitation and evaporation are included in the water mass and salinity balance computation. Wind speed and direction, air temperature and sea surface pressure data were from the NOAA Thomas Point Buoy (38°53′56″ N 76°26′9″ W) located in the northern part of the Chesapeake Bay close to the Chester River Estuary. All other surface forcing data were downloaded from the NARR (North America Regional Reanalysis) ftp site (ftp://ftp.cdc.noaa.gov/Datasets/NARR). NARR provides data at 3-h intervals and linear interpolation was conducted during the simulation.

Fall line data of river discharge was generated by using the USEPA CBP (Chesapeake Bay Program) regulatory watershed model HSPF (Hydrological Simulation Program – FORTRAN). The annual average discharge to the Chester River domain ranges from 13.2 m^3s^{-1} in 2007 to 31.5 m^3s^{-1} in 2003. As such, 2007 is the driest year and 2003 the wettest year during the simulation period (Fig. 2). Linear interpolation was performed on the daily river discharge data during the simulation.

Open boundary forcing data of sea surface elevation, temperature and salinity are computed by the EPA CBP regulatory hydrodynamics model CH3D. CH3D simulation was first conducted for the entire Chesapeake Bay using the same watershed model outputs of river discharges from 2002 to 2011. The physical fields of temperature, salinity and surface elevation at the Chester River mouth nodes were extracted for the open boundary condition for the Chester River Estuary simulation. The FVCOM Chester River Estuary grid was thus designed that the open boundary nodes are exactly at the CH3D nodes and, consequently, horizontal interpolation was not needed. CH3D uses the z-coordinate in the vertical and its number of layers differ between nodes depending on the total water depth. Vertical linear interpolation was conducted to convert the output of CH3D to the sigma levels of FVCOM. Linear interpolation was also conducted for each FVCOM simulation time step between the hourly outputs of CH3D. Jiang and Xia (2016) and Xia and Jiang (2016) have applied FVCOM to the entire Chesapeake Bay, which can provide open boundary forcing for tributary simulation in the future.

Sea surface elevation at the open boundary shows considerable seasonal and interannual variations in addition to semi-diurnal and diurnal tide cycles (e.g., M2 and S1 constituents; Fig. 3). Sea surface elevation tends to be higher during the summer and spring seasons than in winter and fall. Harmonic analysis of the open boundary sea surface level revealed that within a monthly time scale, M2 (Principal lunar) constituent contributes 49% to the total tidal energy spectrum, and the fortnightly constituent (MSF) 38%, followed by K1, O1 and Q1, which constitute the top five tidal constituents. On an annual basis, the solar semiannual constituent (SSA) constitutes the second to M2 in the tidal energy spectrum (Table 1). On long-term multi-year time scales, the solar annual constituent (SA) constitutes the second tidal constituents and SSA becomes the third. Apart from the semi-diurnal M2 tide, the annual and semiannual low frequency tidal constituents are significant in the Chester River and Chesapeake Bay.

2.3. Observation data

The Chesapeake Bay Program (CBP) maintains a monitoring program over the entire Bay since 1984. Two of the long-term monitoring stations are in the Chester River domain: ET4.2 in the lower estuary and ET4.1 in the upper estuary (Fig. 1). Data of temperature and salinity from monthly (in winter) and biweekly (in summer) cruises are available for the entire simulation period from 2002 to 2011 (Fig. 4). DNR (Department of Natural Resource, MD) also undertakes monitoring activities in the Maryland portion of the Bay including the Chester River and the Corsica River in the simulation domain. Some of the stations were occupied in long terms such as XGG8251 located on the southern bank of the Chester River Estuary (Fig. 1), but most of the DNR monitoring stations are rotational, occupied in different years. There are 23 stations sampled during the simulation period in the DNR monitoring programs (Fig. 4).

In addition to cruise-based monitoring programs, DNR conducted Continuous Monitoring programs (CMON) at nine of the monitoring stations (Solid line in Fig. 4). These are high-frequency (every 15 min) data based on electronic sensor and tele-communicated to land-based laboratories. The sensors were carefully calibrated on a monthly basis with bottle sample analysis. Due to the large quantity of data available to this study, only a subset will be presented in the following sections, whereas all the data were included in the statistical analysis, such as the Taylor and Target diagrams.

2.4. Statistical analysis

Taylor diagram, Target diagram, General Additive Model (GAM) and Principal Component Analysis (PCA) were used to analyze the simulated results together with observation and forcing data. Briefly, Taylor diagram depicts comparison between the simulation and observation in terms of correlation coefficient, standard deviation of both simulation and data and centered root mean square error (CRMSE) on the same diagram (Taylor, 2001). The fundamental algorithm is the following:

$$\sigma_x^2 = \frac{1}{N}\sum_n^N (x_n - \bar{x})^2 \quad (1)$$

$$\sigma_y^2 = \frac{1}{N}\sum_n^N (y_n - \bar{y})^2 \quad (2)$$

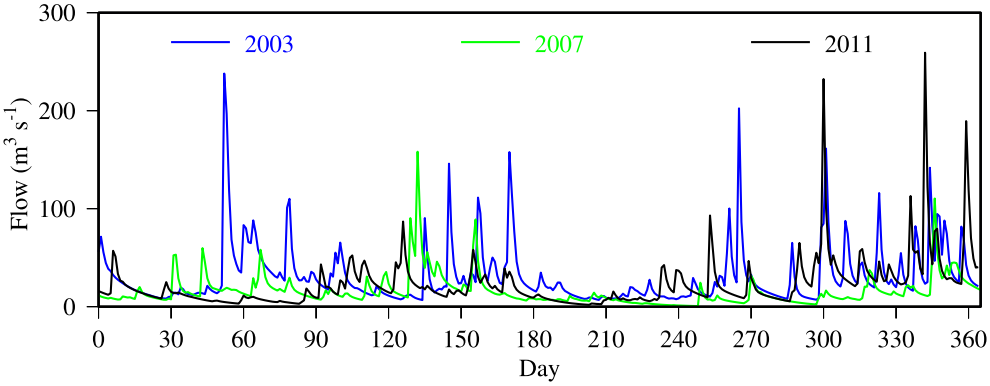

Fig. 2. Daily river discharge in 2003 as a wet year, 2007 as a dry year and 2011 with storm events in the fall.

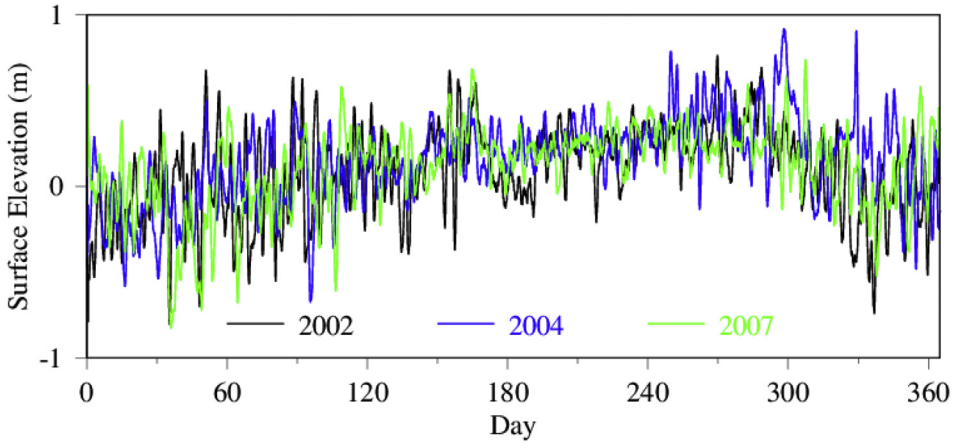

Fig. 3. Sea surface elevation at the central node of the open boundary of 2002, 2004 and 2007.

Table 1
Top 5 tidal constituents from harmonic analysis of the open boundary sea surface elevation (Tidal constituents: K1: Luni-solar declinational (23.92d); M2: Principal lunar (12.42h); MSF: Lunisolar synodic fortnightly (14.78d); O1: Principal lunar diurnal (25.82h); Q1: Larger lunar elliptic diurnal (26.87h); SA: Solar annual (365.26d); SSA: Solar semiannual (182.62d).

Analysis	Constituents	Amplitude (m)	Percent energy
Monthly	M2	0.15	49
	MSF	0.13	38
	K1	0.05	6
	O1	0.04	4
	Q1	0.03	2
Annual	M2	0.17	52
	SSA	0.12	24
	K1	0.06	6
	MSF	0.05	5
	O1	0.05	5
Multi-years	M2	0.17	39
	SA	0.16	34
	SSA	0.09	11
	K1	0.06	5
	O1	0.05	4

$$R = \frac{\frac{1}{N}\sum_{n}^{N}(x_n - \bar{x})(y_n - \bar{y})}{\sigma_x \sigma_y} \tag{3}$$

$$E^2 = \frac{1}{N}\sum_{n}^{N}\left[(x_n - \bar{x}) - (y_n - \bar{y})\right]^2 \tag{4}$$

where E, R, σ, x and y are the centered root means square error, correlation coefficient, standard deviation of simulation and data, respectively and the overbar indicates the mean. The key algorithm is that E is related to R and σ by:

$$E^2 = \sigma_x^2 + \sigma_y^2 - 2\sigma_x\sigma_y R \tag{5}$$

where R is expressed by the inverse cosine of the azimuthal angle and σ by the radius in the Taylor diagram, E turns to be the distance between the data and the simulation (see the "Result" section for illustration). Due to the different unit of variables, the standard deviation of simulation is normalized to that of the observation so that the radius unit is the data standard deviation (Jolliff et al., 2009; Tian et al., 2014).

The Taylor diagram does not give the total bias or the total root mean square error between the data and the simulation. The total mean square error (MSE) can be described as the sum of the centered mean square error (also called unbiased mean square error) and the squared bias defined as the difference of the mean between the simulation and data (Jolliff et al., 2009):

$$MSE = E^2 + B^2 \quad where \quad B = \bar{x} - \bar{y}. \tag{6}$$

In the Target diagram, the bias is scaled on the x axis and the centered mean square error on the y axis and, as a result, the total bias is the radial distance from the origin to the data point. The combined Taylor and Target diagram can thus give a relatively comprehensive assessment of the simulation by providing the correlation coefficient, standard deviation of both data and simulation, the centered mean square error, the bias and the total MSE (See "Result" section below for graphic examples).

General linear model is based on the assumption of normal distribution of the data, which may be violated in certain cases. Generalized linear model alleviates that assumption by dealing with different distributions, but its application can be limited by the specific

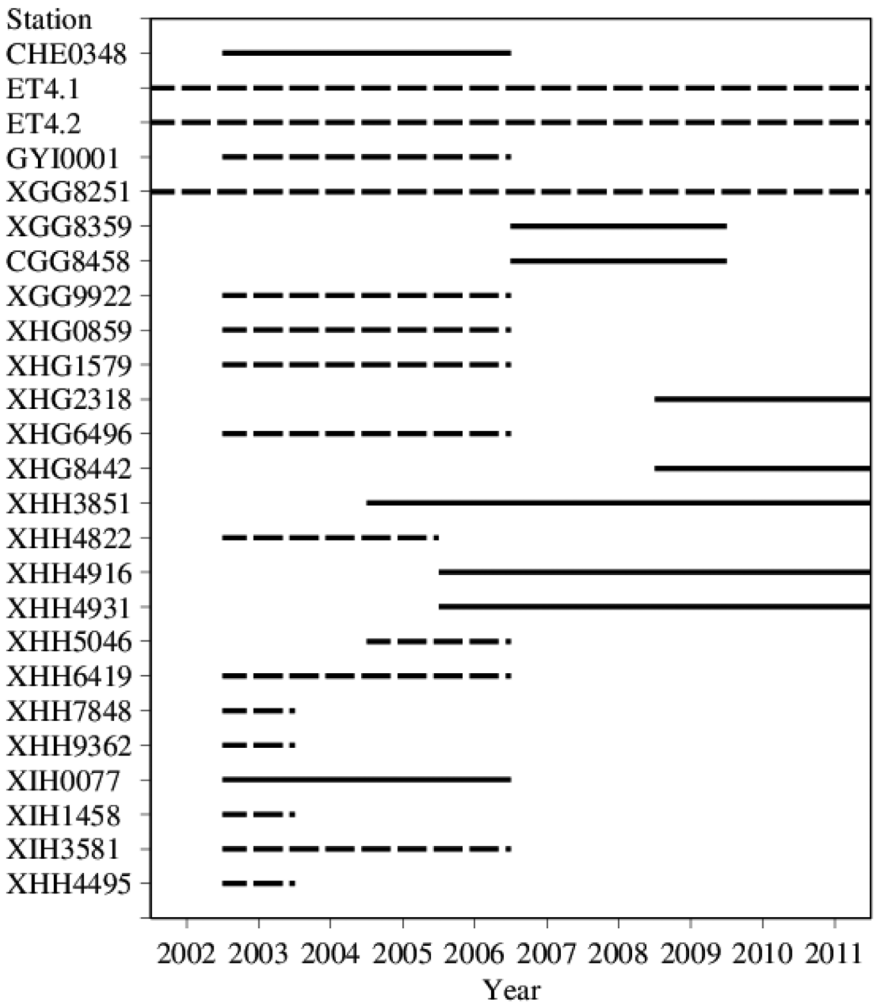

Fig. 4. Monitoring stations and data availability for temperature and salinity. Dash line indicates cruise-based biweekly and monthly data and continuous line indicate Continuous Monitoring (CMON) data collected with electronic sensors at a 15 min interval.

distribution, parametric fitting and linear responses. Generalized additive model (GAM) takes a nonparametric approach without specific distribution assumption and local fitting of different predictive variables. Low-pass filter is often used in saltwater intrusion studies to remove high-frequency variations due to semi-diurnal and diurnal tides (Perales-Valdivia et al., 2018; Guerra-Chanis et al., 2019), but it does not separate variations on different time scales such as seasonal and interannual variability. Harding et al. (2015) found that GAM is suitable to analyze time series data, discern long-term trend, interannual and seasonal variability, which was adopted in this study. For the interannual variability, the model in R is:

$$y = \text{gam}(s(\text{time}, bs = \text{"cr"})) \quad (7)$$

where *y* is a variable to be analyzed, time expressed decimal years since 2002 and *"cr"* indicates that "cubic spline" method is used in the smoothing process. The model for seasonal variability is:

$$y = \text{gam}(s(\text{DOY}, bs = \text{"cr"})) \quad (8)$$

where *DOY* stands as "Day of the Year" ranging from 0 to 365 (366 for leap years) for each year, and the model for the combined variability is:

$$y = \text{gam}(s(\text{time}, bs = \text{"cr"}) + s(\text{DOY}, bs = \text{"cr"}) + ti(\text{time}, \text{DOY}, bs = \text{"cr"})) \quad (9)$$

where *ti* is the tensor product interaction function of time and DOY.

Principal component analysis (PCA) is a common method in statistical analysis. It is a type of linear transformation through which principal dimensions are found in the variable space. This is achieved through eigenvalue decomposition and the correlated variables are grouped on their common eigenvector (principal component axis) which explains their common variance (Gotelli and Ellison, 2004). In our case, different variable units can potential influence the PCA result. To overcome this potential bias, normalization or correlation coefficient are used. In this study, the correlation coefficient matrix is used to build the principal component axes. As this paper focuses on variations of saltwater intrusion over difference time scales, GAM was first applied to the raw data to extract signals on seasonal and interannual time scale. The extracted data were then analyzed using the PCA function in the R package FactoMineR.

3. Result

3.1. Comparison between simulation and observation

Data of temperature and salinity collected at 25 stations were used to assess the robustness of the simulation. Although this paper focuses on saltwater intrusion, estuarine circulation is primarily driven by the density field determined by both temperature and salinity. Consequently, temperature and salinity are both presented in this section. Given the large quantity of data, only the most representative stations are illustrated in detail: ET4.1 and ET4.2 with the longest time series data over the entire simulation period, and XHH3851 with the longest record of continuous monitoring data from 2005 through 2011

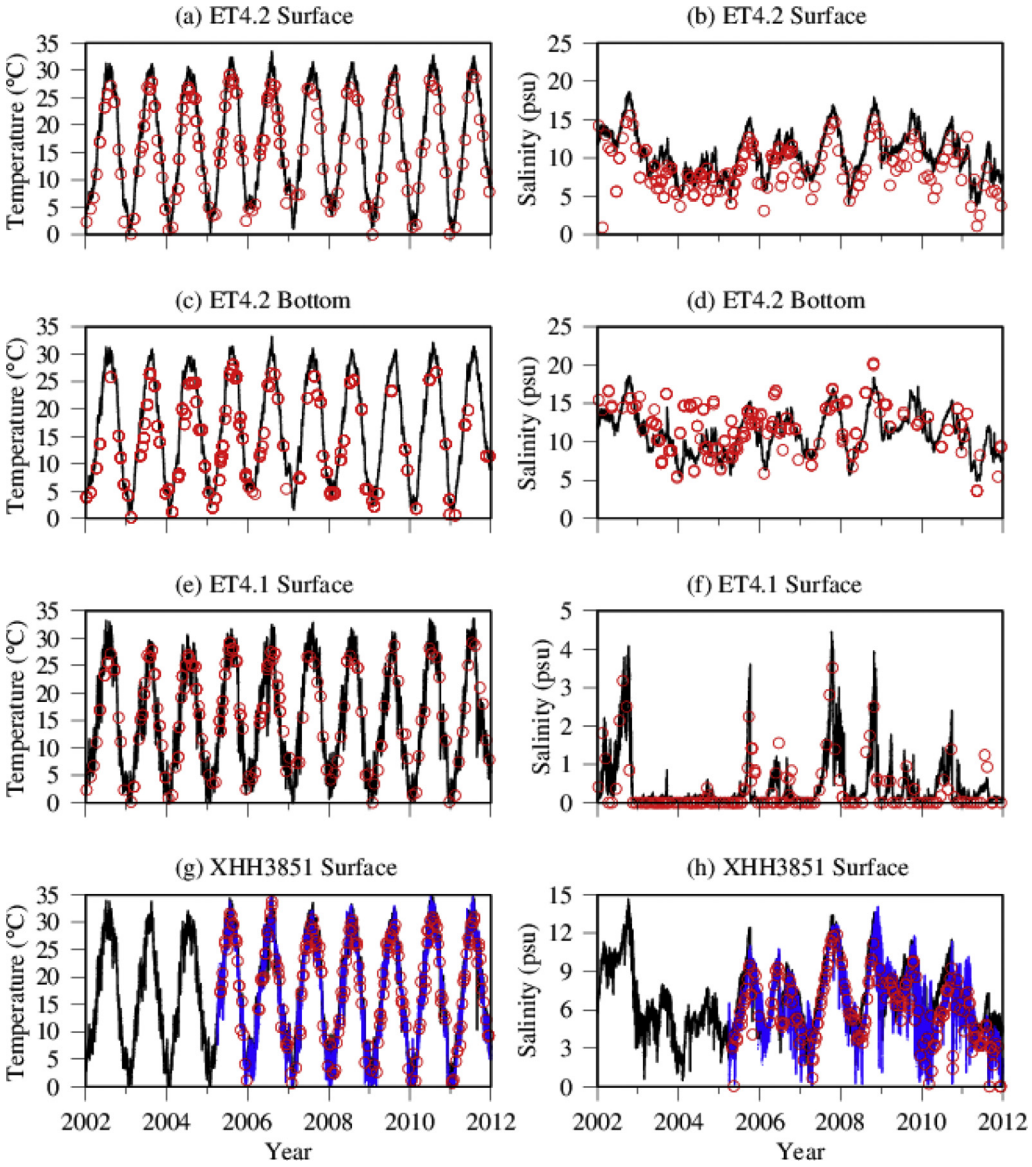

Fig. 5. Comparison of simulated temperature and salinity (black lines) with data (red circles for cruise data and blue lines for continuous monitoring data) at Station ET4.2 in the lower estuary mesohaline region (salinity 5-18psμ), ET4.1 in the upper estuary tidal fresh zone (salinity < 0.5 psμ during most of the time), and XHH3851 in the Corsica River. Both the surface and bottom layers are shown at the deep station ET4.2 whereas only one layer (surface) shown at the shallow stations ET4.1 and XHH3851. (For interpretation of the references to colour in this figure legend, the reader is referred to the Web version of this article.)

(Fig. 5). Data from other stations were included in the statistical analysis for the Taylor and Target diagrams.

Station ET4.2 is in the deep lower estuary (Fig. 1). The simulated temperature in both surface and the bottom layers match the data in terms of absolute values, seasonal and interannual variations (Fig. 5 a and c). In the winter of 2003, 2004 and 2011, water temperature fell to 0 °C in both the surface and the bottom layers. In the winter of 2006 and 2008, however, water temperature remained above 5 °C. In most cases, surface water temperature is higher than that in the bottom layer, but in the winter of 2009, the surface water temperature was slightly lower than that in the bottom layer, resulting a reversed temperature gradient in the water column. All these observations indicate significant interannual variations in both simulated and observed temperature in the Chester Estuary. The salinity at this station mostly ranges from 5 to 18 p.s.u., within the mesohaline salinity range (Montagna et al., 2013). Both observation and simulation show considerable seasonal variations (Fig. 5 b and d). Salinity tends to be lower in later winter and spring and higher in fall. In 2004, however, the salinity remained at a relatively lower level year-round, whereas the highest salinity up to 18 p.s.u. was observed and simulated in fall 2002, 2007 and 2008. In most cases, salinity simulation agrees with the observation. Salinity data in the bottom layer in 2004 are relative scattered and the model simulation is at the low end of the observed salinity range.

Station ET4.1 is in the upper estuary with salinity lower the 0.5 p.s.u. during most of the time (tidal fresh zone; Montagna et al., 2013). It is a shallow station (3 m deep) so that only the surface layer is presented in Fig. 5 (e and f). Temperature simulation and observation have a similar range from 0 °C in winter and around 30 °C in summer. On an interannual scale, 2006 had the warmest winter during the simulation period. The most striking phenomenon is the salinity distribution (Fig. 5 x and f). Salinity intrusion barely reached to this station in some of the simulated years (i.e. 2003, 2004 and 2011), but salinity concentration reached up to 4 p.s.u. in late fall 2002, 2005, 2007 and 2008, and about 1–2 p.s.u. in 2006, 2009 and 2010. Almost every time the observation revealed a saltwater intrusion event did the model predict a corresponding peak in salinity, comparable in the timing and amplitude. This good agreement between observation and simulation indicates that the model-predicted saltwater intrusion in the upper estuary is robust,

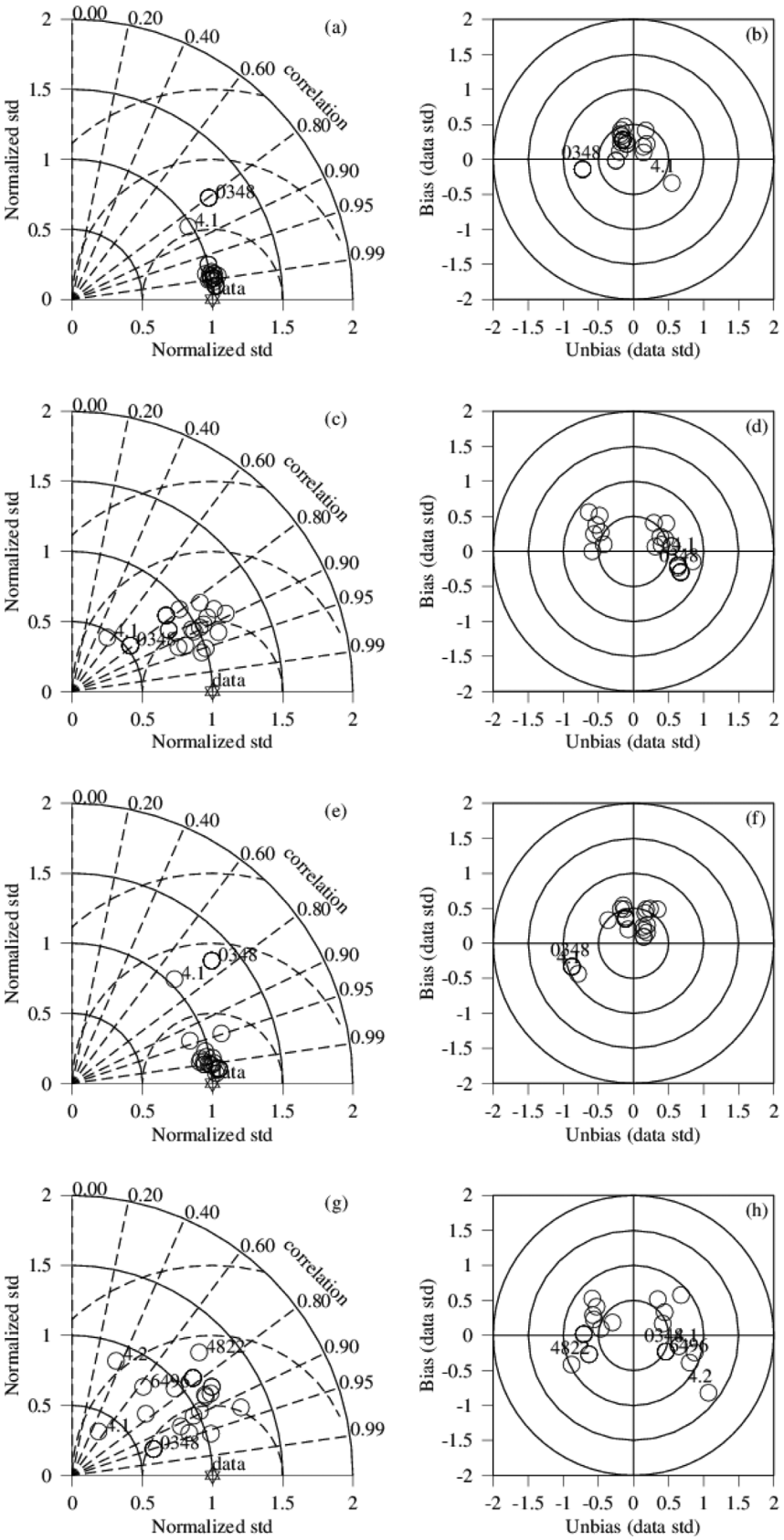

Fig. 6. Taylor (left) and Target (right) diagrams constituted between modeled and observed data over all the stations: (a) and (b) for surface temperature, (c) and (d) bottom temperature, (e) and (f) surface salinity and (g) and (h) bottom salinity.

which constitutes the focus of this paper.

Given the larger quantity of observation data, the Taylor and Target diagrams were used to summarize the statistics between the simulation and observation (Fig. 6). For surface temperature (Fig. 6 a), most of the stations have a correlation coefficient higher than 0.95 between observation and simulation with a centered root mean squared error (CRMSE) close to the standard deviation of the data. As such, most of the stations are clustered close to the data point on the Taylor diagram. Similarly, on the Target diagram (Fig. b), most of the stations are clustered toward the center within the range of a half of the data standard deviation. Stations ET4.1 and CHE0348 have a relatively larger deviation as compared to other stations, but the correlation coefficients and bias are within a plausible range, with a r between 0.8 and 0.85 and a bias lower than the data standard deviation.

For surface salinity (Fig. 6 c and d), the correlation coefficients are mostly higher than 0.8 and the biases and CRMSE lower than the standard deviation of the data. These numbers slightly lower than that for surface temperature, but within a reasonable range as model-data comparison. Again, stations ET4.1 and CHE0348 are further away from the cluster of other stations, indicating a relatively poor data-model comparison. The correlation coefficient of surface salinity is about 0.5 for ET4.1 and 0.8 for CHE0348, but the biases are all within the standard deviation of the data. These two stations are in the tidal fresh zone where relatively large variations can occur due to interannual variations in saltwater intrusion and sporadic events in weather and river discharge. As can be seen in the detailed data-model comparison in Fig. 5, major saltwater intrusion events were reproduced over a decadal time scale by the model.

Similar results were obtained for the bottom temperature simulation (Fig. 6 c and d). Most of the stations have a correlation coefficient higher than 0.95 and a total bias lower than the standard deviation of the data. Station ET4. 1 and CHE0348 are separated from the rest of the stations, with the correlation coefficient around 0.75 and total bias close to 1 standard deviation of data. Salinity in the bottom layer shows more scattering than in the surface layer (Fig. 6 g and h). In addition to Station ET4.1, Station ET4.2 also shows relatively poor model-data comparison as compared to other stations. The total bias of bottom salinity at Station ET4.2 is higher than the standard deviation of the data (close to one and a half times the data STD) with R close to 0.4. As we mentioned earlier (Fig. 5 f), a wide range of salinity values were reported in 2004 and the model reproduced the low end of the observation. This appears to be the main cause of the poor model-data statistics for the bottom salinity at this Station. As saltwater intrusion was not observed nor simulated in 2004, this model-data deviation did not appear to significantly influence the outcome of saltwater intrusion simulation in the upper estuary.

3.2. Saltwater intrusion

Salinity of 2 p.s.u. has been used to define the saltwater intrusion limit in estuaries (Monismith et al., 2002; Pinho and Vieira, 2007; Yoon and Woo, 2013; Guerra-Chanis et al., 2019). The total length of the simulation domain is 65 km and the 2 p.s.u. reached to the upstream boundary in some occasions. As such, the 2 p.s.u. limit is no more an accurate measure for the interannual variations of saltwater intrusion. Consequently, 5 p.s.u. was used to measure the changes in saltwater intrusion distance, i.e. the distance from the estuary mouth to the 5 p.s.u. isopleth on an hourly basis. Although the absolute value of saltwater intrusion extent should be larger if determined by 2 p.s.u. than by 5 p.s.u., the variability between the two should be correlated.

Saltwater intrusion shows considerable seasonal and interannual variability, but the diurnal variation due to tide is relatively limited (Fig. 7 a). Based on harmonic analysis, all the tidal constituents with a period smaller than 25 h contribute to 2.86 km in the variations of saltwater intrusion extent in the surface layer and 1.27 km in the bottom layers. The larger amplitude in the surface layer as compared to the bottom layer is most likely due to amplification by river discharge. Alternatively, averaged diurnal variability of saltwater intrusion extent (the maximum minus the minimum with 25 h) is 2.58 km in the surface layer and 1.36 km in the bottom layer. The two estimates are in good agreement and show that changes in the saltwater intrusion due to semidiurnal and diurnal tides is below 3 km in the surface layer and below 1.5 km in the bottom layer.

Saltwater intrusion shows larger variations on seasonal than on diurnal time scales. In most of the simulated years, saltwater intrusion tended to be weaker (with short intrusion distance) during the spring season than in the fall. In 2005 and 2007, for example, saltwater intrusion reached to about 30 km from the river mouth in winter, but to 63 km in the fall, i.e. a seasonal variation over 30 km. However, the seasonal variation differs between years, indicating important interannual variations. In the winter of 2004, saltwater intrusion reached to only 20 km from the mouth, about 10 km shorter than other years. Also, the peak intrusion in fall reached only to 45 km, considerably shorter than in other years. In 2003, saltwater intrusion had limited seasonal variations, varying only from 40 to 50 km without noticeable minimum in the winter-spring season.

The difference in saltwater intrusion between the bottom and surface layers can reflect the strength of the two-layer estuarine circulation. The difference between bottom and surface saltwater intrusion ranged from 0 to 11 km with a global average of 2.3 km. There is a significant relationship between bottom-surface difference and the saltwater intrusion distance (Fig. 7 b). The global relationship with all daily data has a negative slope of -0.13 and correlation coefficient of 0.66 ($n = 3652$). Interesting is that there are three segments in the saltwater intrusion distance within which relationship differs. When the total saltwater intrusion is shorter than 32 km in the lower estuary, the relationship slope is as larger as -0.49 (with correlation coefficient of 0.72). This distance range covers up to Corsica River where the estuary channel is considerable wider and deeper than in the upstream segments (Fig. 1). The second segment ranges from 32 to 54 km between Station XIH1458 and 0077 in the mid-estuary where the relationship between the bottom-surface difference and total saltwater intrusion distance has a slope of -0.11 and correlation coefficient of 0.44, lower than that in the lower estuary. Above the 54 km limit is a shallow narrow channel in the upper estuary where there is no significant difference between the bottom and surface layer saltwater intrusion (only 0.7 km in average). It is noteworthy that the second segment mentioned above is fragmented into several small segments between which the relationship is interrupted. There is strong relationship in each subsegment, but the difference between bottom and surface saltwater intrusion is considerably reduced at the boundaries, which are coincident with the meanders of the channel. The curvatures reduce the surface-bottom difference in saltwater intrusion and thus limit the development of the two-layer circulation.

For long-term variability analyses, diurnal variations were first removed by calculating the daily average (25 h average given the semidiurnal tide period of 12.42 h), then the GAM was applied to the daily data to determine the interannual, seasonal and combined variability (Fig. 8). These analyses were performed to both surface and bottom saltwater intrusion distance. Given the similarity in terms of variations, only the result of the surface layer is presented. The interannual variability explains 38% of the total variance. Saltwater intrusion tended to decrease from 2002 to 2004 to reach to a minimum in the winter 2004, then gradually increased from 2004 to 2009, followed by a decreasing trend till the end of the simulation in 2011. The amplitude of the long-term variation is about 20 km over the simulation period.

The seasonal variation fitted by the GAM represents an average over the simulation period (Fig. 8 green line). The fitted seasonal variability explains 19% of the total variance. The general pattern is lower in the winter and early spring seasons and higher in later summer and early fall. The amplitude of the fitted seasonal variation is about 10 km. With the interannual and seasonal variability combined (Fig. 8 red line), the

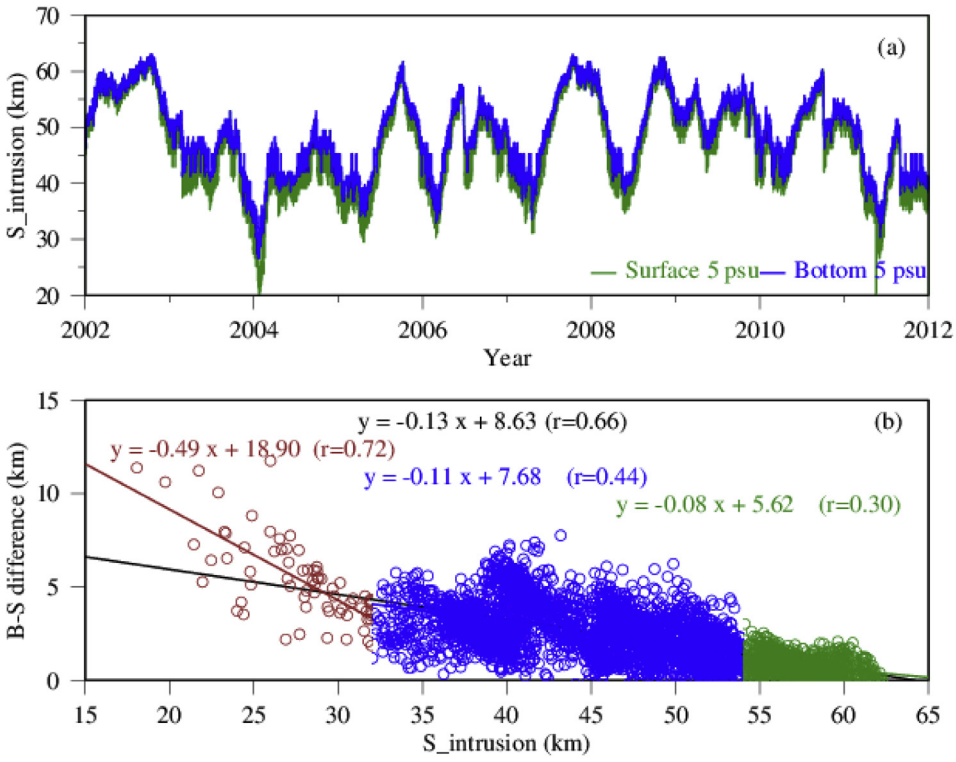

Fig. 7. (a) Hourly simulated salt water intrusion distance (S_intrusion) demarcated by the 5 p.s.u. limit in both the surface (green) and bottom layers (blue) and (b) relationship between the difference (bottom minus surface salt water intrusion distance) and surface saltwater intrusion. Black line and equation are based on the ensemble data, brown for saltwater intrusion lower than 32 km, blue for saltwater intrusion between 32 and 54 km and green for saltwater intrusion greater than 54 km. (For interpretation of the references to colour in this figure legend, the reader is referred to the Web version of this article.)

fitted model explains 82% of the total variance and show large variations on the interannual scale. At the low end of the spectrum (the minimum of saltwater intrusion extent), the fitted low value is only 25 km in 2004, but 47 km in 2009, i.e. an interannual variation over 22 km. At the high end of spectrum, the fitted model generated values of 62 km in 2007, but only 42 km in 2011, a 20 km interannual difference as well. In addition to the interannual variations in the amplitude of saltwater intrusion, the timing of the seasonal sequence varies on an interannual scale as well. Instead in late winter and early summer as in general and predicted by the GAM seasonal model, the minimum salt water intrusion distance occurred in early winter 2003 through 2005, resulting in a skewed pattern toward the early season at the low end of the spectrumrange.

4. Discussion

It is relatively well documented that sea surface level, river discharge and wind are the potential factors controlling the variation in saltwater intrusion in estuaries, but reports on the relative dominance among the controlling factors across time scales are scarce. We will start the discussion on the long-term interannual variations, through the seasonality to short term event-related variations. A concern for wind is that not only wind speed, but also wind direction can affect the saltwater intrusion intensity. The geometry of the Chester River Estuary is relatively meandering (Fig. 1). Nevertheless, from the mouth to Station XHG1579 in the lower estuary, south-north and west-east direction dominating. From the mid estuary to the upper estuary, the major channel runs mostly northeastward. In order to taken into account both wind direction and speed, wind was projected on to four directions:

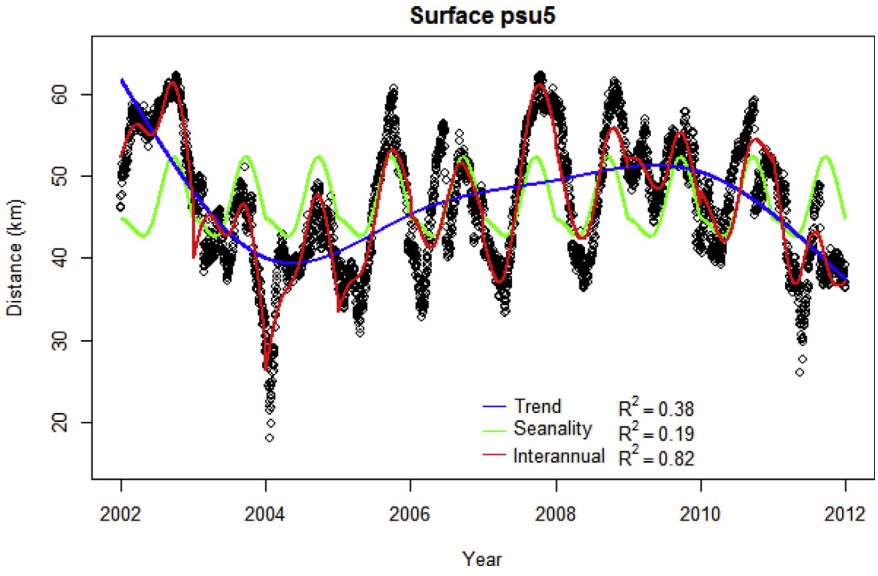

Fig. 8. GAM analysis of saltwater intrusion distance in the surface layer determined with the 5 p.s.u. limit. The interannual variability (blue line) explains 38% of the total variance, seasonal variability (green line) 19% and the combined variability (red line, including interannual and seasonal variations) up to 82% of the total variance. (For interpretation of the references to colour in this figure legend, the reader is referred to the Web version of this article.)

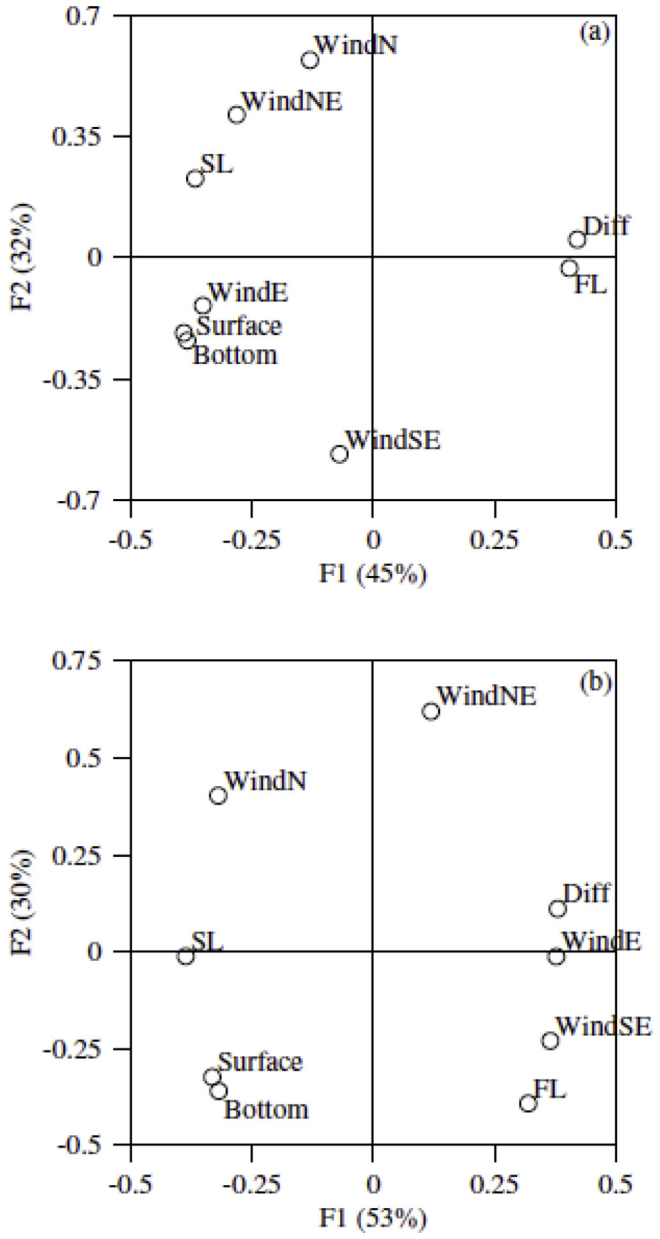

Fig. 9. Principal component analysis (PCA) of saltwater intrusion distance with forcing variables: (a) Interannual variability PCA and (b) seasonal variability PCA. Bottom: Bottom saltwater intrusion distance; Diff: Difference between bottom and surface saltwater intrusion distance; FL: River flow; SL: Sea surface level at the estuarine mouth; Surface: Surface saltwater intrusion distance; WindE: Eastward wind; WindN: Northward wind; WindNE: Northeastward wind; WindSE: Southeastward wind.

south-north (WindN); west-east (WindE) and southwest-northeast (WindNE); northwest-southeast (WindSE). The south-north west-east wind is perpendicular or along the lower estuary and the other pair are perpendicular to or along the upper estuary.

GAM analysis was performed on all the potential factors to extract long-term interannual trend and seasonal variations and principal component analysis was conducted separately on each constituent. For the long-term trend, the first and the second principal components explain about 77% of the total variance and thus quite representative of the variables analyzed (Fig. 9 a). Saltwater intrusion in both the bottom and surface layer and their difference are mainly loaded on the first principal component whereas WindN, WindNE and WindSE are mostly projected on the second principal component. Consequently, the first principal component can be considered as the saltwater intrusion axis (PC1) and the second the wind axis (PC2). The saltwater intrusion distance in both the bottom and surface layers are on the negative side of PC1 whereas their difference on the positive side, indicating their opposite variations. River flow (FL) is closely related to the bottom-surface difference on the positive side of PC1, opposing saltwater intrusion distance on the negative side, indicating that river flow is a dominant factor in determining the long-term interannual variations in saltwater intrusion. High river flow results in weak saltwater intrusion, but larger difference between the bottom and surface layer and thus stronger two-layer estuarine circulation. Theoretically, saltwater intrusion and the two-layer estuarine circulation do not have a linear relationship with the flow (Snedden and Xu, 2016; Perales-Valdivia et al., 2018). When river flow is weak, tide and tidal mixing dominates so that stratification and the two-layer gravitational circulation are restricted. Too strong river discharge will flush salt water out of the estuary and the two-layer gravitational circulation cannot form neither. Moderate flows favor the most the two-layer estuarine circulation. However, the Chester River Estuary is a complex system. The upper estuary is a shallow narrow channel where the development of two-layer circulation is limited and the saltwater moves forth and back following river discharge and tidal forcing without distinct different between surface and bottom layer. In the mid-estuary where water depth is sufficiently deep for the development of two-layer circulation, the meandering restricts the development of two-layer circulation to certain degree. Stratification and difference between surface and bottom saltwater intrusion develop between curvatures, but at the curvatures, the two-layer system is reduced. Channel curvature and meanders can alter both lateral and along channel circulation through centrifugal force and helical lateral flow and, consequently, reduce the two-layer circulation and stratification (Lacy and Monismith, 2001; Chant, 2002; Basdurak and Valle-Levinson, 2013). The Rossby number is used to describe the ratio or balance between the inertial force and the Coriolis force. For stream curvatures where centrifugal force becomes the dominating inertia, the Rossby number (Ro_R) is defined based on the radius of the curvature R:

$$\mathrm{Ro_R} = \mathrm{U/Rf} \tag{10}$$

where U is the current and f is the Coriolis coefficient (Chant, 2002; Cossu and Wells, 2010; Wells and Cossu, 2013). Lower Rossby number ($Ro_R < 1$) means Coriolis force dominating and higher Rossby number indicates centrifugal force prevails. The Coriolis coefficient at the Chester Estuary latitude (39° N) is $f = 2\Omega\sin(\varphi) = 2\bullet\ 7.2921 \times 10^{-5} \bullet\sin(39) = 9 \times 10^{-5}$, and the radii of the curvatures between Station XHH7848 and XIH0077 are approximately 1000 m (Fig. 1). Current at these stations reaches to 60 cm s^{-1}, yielding an R_{OR} about 7, well within the range of centrifugal dominance.

With high loading on the first PC1, sea surface level (SL) is the second dominating factor in determining the saltwater intrusion distance and the two-layer estuarine circulation on an interannual time scale. However, sea surface level loaded on the negative side of PC1, opposing the river discharge loaded on the positive side. Higher sea surface level leads to longer saltwater intrusion, but smaller bottom-surface difference and thus weaker two-layer gravitational circulation.

East Wind (WindE) is ranked the third in terms of loading on PC1 (Fig. 9 a). High eastward wind leads to stronger saltwater intrusion, but smaller bottom-surface difference and weaker two-layer circulation. On the other hand, north and south-east winds are mostly projected on PC2, i.e. perpendicular to the saltwater intrusion axis and thus have little influence. As eastward wind is mainly along the estuary, wind strain appears to be more important than the Ekman transport. Three factors may help to explain this observation: (1) The shallow depth in the upper estuary restrict the development of the Ekman layer (Chen et al., 1996); (2) Narrow channel also limits the wind fetch and the extent of the Coriolis forcing effect; (3) Stratification, essentially in the

lower estuary, reduces momentum transfer from the surface to deep layers, upon which the Ekman transport develops (Price et al., 1987; Price and Sundermeyer, 1999). As a result, along channel wind has a stronger effect on saltwater intrusion than cross-channel wind in the Chester River Estuary, in agreement with previous studies in other estuaries (Lips et al., 2017; Liu et al., 2019).

For seasonal variations in saltwater intrusion and two-layer gravitational circulation (Fig. 9 b), the first principal component explains 53% of the total variance and thus represents the major component and the second principal component accounts for 30% of the total variance. Saltwater intrusion distance in both the surface and bottom layer are in the third quadrant, opposing to the difference between the two layers located in the first quadrant. If the principal component axes are rotated counterclockwise by about 45°, the rotated axis from the third quadrant to the first quadrant constitutes the saltwater intrusion axis and the second and the fourth quadrant axis consist of wind variables. Sea surface level becomes the top explanatory variable for the seasonality in saltwater intrusion, whereas river flow is the primarily explanatory variable to long-term interannual variability. Wind has relatively less influence on saltwater intrusion on the Chester River Estuary as the seasonal variability is concerned. North and Southeast wind constitute the second-fourth quadrant axis perpendicular to the saltwater intrusion axis and thus lack of correlation with the seasonal variation in the saltwater intrusion. The loadings of East and Northeast winds are also relatively low on the principal components, indicating that wind only has minor influence on seasonal variations of saltwater intrusion in the Chester Estuary.

4.1. Event based analysis

Saltwater intrusion extended to the tidal fresh zone mostly in late summer and fall and particularly in 2005, 2007, 2008 and 2010. Summer 2007 is presented as an example (Fig. 10 a) when the 5 p.s.u. isopleth gradually moved about 20 km upstream. This shows that the extension of the saltwater intrusion to the tidal fresh zone is a seasonal dispersive phenomenon (Fischer, 1972; Kuijper and Van Rijn, 2011). Geyer and Signell (1992) found that the dispersive transport of salt is controlled by the tidal excursion and geographic features. The tidal excursion is very short and the main channel featured with many meanders which can lead to slow upstream propagation of salt to the upper estuary. The most striking feature in the forcing data is the extreme low river fresh water flow during the summer 2007. There is no well-defined pattern in the wind forcing so that it is unlikely that wind significantly contribute to the seasonal upstream extension of saltwater intrusion. There is no clear trend in the sea surface level forcing neither.

Although the extension of saltwater intrusion to the tidal fresh zone are gradual seasonal events, the retreat of saltwater can occur rapidly, within a few days. Fall 2011 is presented as an example in Fig. 10 b. It can be observed that saltwater intrusion retreated over 10 km in two days. This retreat corresponds to an intense rain fall event related to the Tropical Storm Lee. On day 239 and 240, 2011, about 60 million cubic meters fresh water emptied into the upper Chester. Assuming an average width of 500 m for the upper Chester (based on GIS estimates), average depth of 3 m and total length of 40 km, this amount of fresh water would flush the entire upper Chester. Under the influence of tide, stratification and two-layer circulation, a great portion of the fresh water discharge flows out in the upper layer. At the same time of the rainfall event, the sea surface level at the Chester River mouth dropped by about 60 cm from 30 cm above to 30 cm below the long-term mean sea surface level, which contribute to the rapid retreat of saltwater intrusion. Note that the sea surface level bounced back after the drop, but saltwater intrusion did not extend in a corresponding manner.

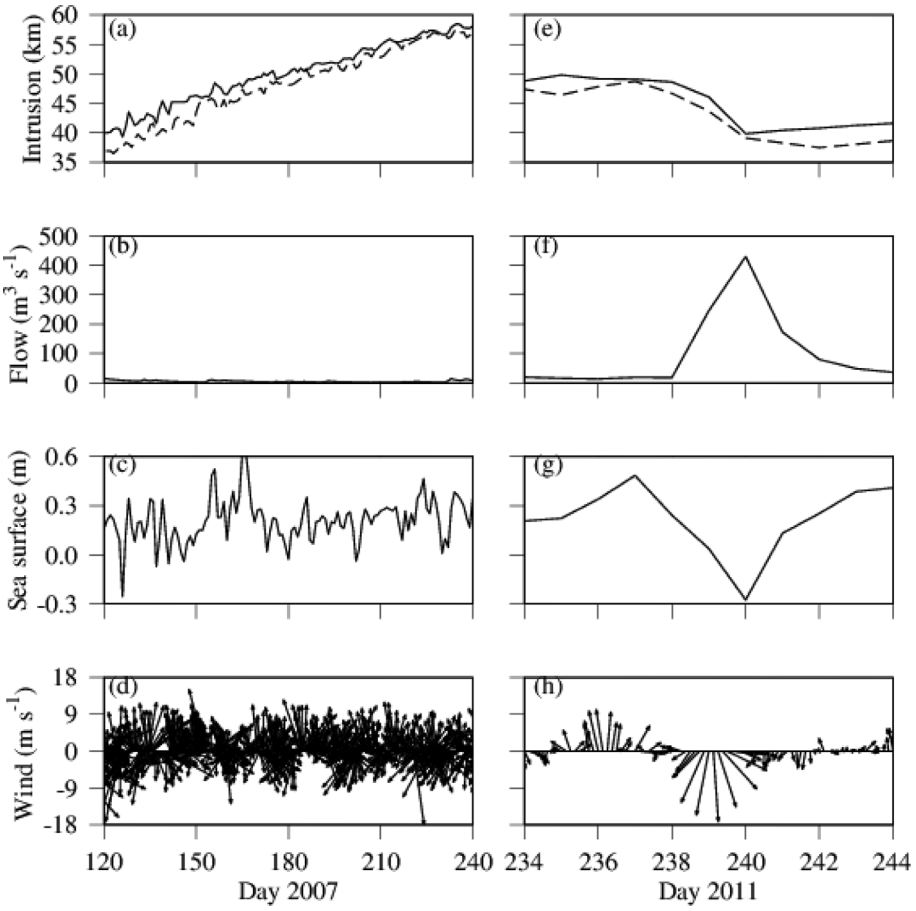

Fig. 10. Saltwater intrusion distance (a, e), river discharge (b, f), sea surface level (c, g) and wind (d, h) in summer 2007 when saltwater intrusion gradually extended from the mid-estuary to the tidal fresh (left panel) and fall 2011 (right panel) when abrupt retreat (within 2 days) from the upper to mid-estuary accompanying with wind, sea level surface and river discharge during the Tropical Storm Lee.

Kuijper and Van Rijn (2011) argued that the response to an increase in river discharge is essentially a flushing process that saltwater is washed out. But the response to a reduction in discharge is mainly a dispersive process that requires a much longer period of time. This is particularly true when the tidal excursion is relatively small.

Strong wind accompanied the rainfall event, with north wind speed up to 24 m per second and wind gust up to 30 m per second (~110 km per hour). With the limited north wind fetch in the Chester, it is unlikely that wind-generated transport can play a major role in the retreat of saltwater intrusion. However, the sea surface level in the Chesapeake Bay and at the mouth of the Chester River is subject to wind forcing and the drop of the sea surface level at the mouth of the Chester River is a response to this strong wind event. Previous studies showed that north-south wind events modulate sea surface level in the Chesapeake Bay and at the mouth of local tributaries (Pollack, 1960; Pasternack and Hinnov, 2003). Elliott (1978) observed that downstream wind stress blew out water from the estuary of the Potomac River, causing a reduction in the local sea surface level and setting increased sea surface slope from the head to the month of the estuary. Chung and Boicourt (1989) revealed that there is a Resonant Seiche Motion in the Chesapeake Bay with period of 2–4 days driven by north-south wind, which is approximately the duration of the tropical storm Lee. It should be point out that the response of circulation and sea surface level in Chesapeake Bay to wind events is complex, depending on wind direction, speed and duration. Wang and Elliott (1978) argued that up-bay wind stress caused water flushing out of the Bay due to Ekman transport in the North Atlantic Coastal region, which pushed water from the coastal region offshore. During the tropical storm Lee, however, a significant drop of sea surface level in the Bay was observed, indicating increased downstream water transport out of the Bay. Wang (1979b) reported that the time scale is a key element in determining the response to wind event in Chesapeake Bay. For time scale < 4 days, local longitudinal wind dominating. For long time scale > 10 days, the response is essentially determined by the North Atlantic coastal sea surface level resulted from Ekman transport. For time scale between 4 and 10 days, local and coastal responses are mostly coupled during cyclone events and sensitive to east-west wind. Concerning the Chester River response to wind event, it is essentially regulated by the Bay's response through the modulation of sea surface level at the Chester River mouth.

5. Conclusion

Saltwater intrusion in estuaries represents a burning topic due to its adverse impact on freshwater resources and ecological function, and this is particularly true under the rising pressure of climate change and sea level rise. Understanding the mechanism and factors controlling saltwater intrusion is critical for mitigation and management. Although a great amount of effort has been devoted to saltwater intrusion studies, few dealt with changes across different time scales. In this study, the 3D hydrodynamic model FVCOM has been applied to long-term time-series data of temperature and salinity collected in the Chester River Estuary, Chesapeake Bay, which allowed to examine the relative dominance of controlling factors across different time scales. Also, the geometrical specifics of the Chester Estuary, meanders and convergency, make it an ideal site for comprehensive analysis across various controlling factors and mechanisms. This study has revealed that relative dominance of controlling factors of saltwater intrusion changes across different time scales. River discharge is the primary factor in controlling interannual variability in saltwater intrusion, but sea surface level prevails in determining seasonal variations. Although wind has limited impacts on interannual and seasonal variations in saltwater intrusion, it has more impact on saltwater intrusion in short time scales, a few days or shorter. The extension of saltwater intrusion to the tidal fresh zone in the upper estuary is found to be a gradual dispersive phenomenon. However, the retreat of saltwater intrusion can be as fast as a weather event within days. The geometry of the Chester Estuary has particular influence on the estuarine circulation and saltwater intrusion. The shallow and narrow upper estuary is vertically mixed with saltwater moving forth and back depending on river discharge, tide and sea surface level. The mid-estuary is characterized with meanders and curvatures, where the centrifugal force and helical circulation can reduce the stratification and the two-layer estuarine circulation. The lower estuary is more stratified with larger difference of saltwater intrusion distance between the surface and bottom layers. Given the generality of estuary dynamics, these findings are mostly applicable to other estuarine systems with similar characteristics.

Declarations of interest

None.

Acknowledgements

The author thanks the Chesapeake Bay Program and UMCES IAN to provide data and funding (CB-75230480) for this project, the Maryland Department of Natural Resource to provide the Continuous Monitoring data, the editor and two anonymous reviewers for their comments and edition in depth. Special thanks go to the Chesapeake Bay Program Modeling Team for their enthusiastic helps, particularly Lewis Linker, Gary Shenk, Ping Wang, Gopal Bhatt, Kyle Hinson, Bill Dennison, Dave Nemazie, Dottie Samonisky and Ken Barton.

Appendix A. Supplementary data

Supplementary data to this article can be found online at https://doi.org/10.1016/j.ecss.2019.04.041.

References

Basdurak, N.B., Valle-Levinson, A., 2013. Tidal variability of lateral advection in a coastal plain estuary. Cont. Shelf Res. 61 (62), 85–97.
Beardsley, R.C., Boicourt, W.C., 1981. On estuarine and continental shelf circulation in the Middle Atlantic Bight. In: Warren, B.A., B.A, Wunsch, C. (Eds.), Evolution of Physical Oceanography. The MIT Press, Cambridge, MA, pp. 198–233.
Burchard, H., Bolding, K., 2001. Comparative analysis of four second-moment turbulence closure models for the oceanic mixed lay. J. Phys. Oceanogr. 31, 1943–1968.
Burchard, H., Schuttelaars, H.H., 2012. Analysis of tidal straining as driver for estuarine circulation in well-mixed estuaries. J. Phys. Oceanogr. 42, 261–271.
Chant, R.J., 2002. Secondary circulation in a region of flow curvature: relationship with tidal forcing and river discharge. J. Geophys. Res. 107 (C9), 3131. https://doi.org/10.1029/2001JC001082.
Chen, C., Reid, R.O., Nowlin, W.D., 1996. Near-inertial oscillations over the Texas-Louisiana shelf. J. Geophys. Res. 101, 3509–3524.
Chen, C.S., Liu, L., Beardsley, R.C., 2003. An unstructured grid, finite-volume, three-dimensional, primitive equation ocean model: application to coastal ocean and estuaries. J. Atmos. Ocean. Technol. 20, 159–186.
Chung, W.S., Boicourt, W.C., 1989. Resonant seiche motion in the Chesapeake bay. J. Geophys. Res. 94, 2105–2110.
Cossu, R., Wells, M.G., 2010. Coriolis forces influence the secondary circulation of gravity currents flowing in large-scale sinuous submarine channel systems. Geophys. Res. Lett. 37, L17603. https://doi.org/10.1029/2010GL044296.
Elliott, A.J., 1978. Observations of the meteorologically induced circulation in the Potomac Estuary. Estuar. Coast Mar. Sci. 6, 285–299.
Fairall, C.W., Bradley, E.F., Rogers, D.P., Edson, J.B., Young, G.S., 1996. Bulk parameterization of air-sea fluxes for tropical ocean-global atmosphere coupled-ocean atmosphere response experiment. J. Geophys. Res. Oceans 101, 747–3764.
Festa, J.F., Hansen, D.V., 1976. A two-dimensional numerical model of estuarine circulation: the effects of altering depth and river discharge. Estuar. Coast Mar. Sci. 4, 309–323.
Fischer, H.B., 1972. Mass transport mechanisms in partially stratified estuaries. J. Fluid Mech. 53, 671–687.
Friedrichs, C.T., 2009. York River physical oceanography and sediment transport. J. Coastal Res. Special Issue 57, 17–22.
Gay, P.S., O'Donnell, J., 2009. Buffering of the salinity intrusion in estuaries by channel convergence. Hydrol. Earth Syst. Sci. Discuss. 6, 6007–6033.
Geyer, W.R., Signell, R.P., 1992. A reassessment of the role of tidal dispersion in estuaries and bays. Estuaries 15, 97–108.
Gotelli, N.J., Ellison, A.M., 2004. A Primer of Ecological Statistics. Sinauer, Massachusetts, pp. 510.
Guerra-Chanis, G.E., Reyes-Merlo, M.A., Diez-Minguito, M., Valle-Levinson, A., 2019. Saltwater intrusion in a subtropical estuary. Estuar. Coast Shelf Sci. 217, 28–36.

Hansen, D.V., Rattray Jr., M., 1965. Gravitational circulation in straits and estuaries. J. Mar. Res. 23, 104–122.
Harding Jr., L.W., Adolf, J.E., Mallonee, M.E., Miller, W.D., Gallegos, C.L., Perry, E.S., Johnson, J.M., Sellner, K.G., Paerl, H.W., 2015. Climate effects on phytoplankton floral composition in Chesapeake Bay. Estuar. Coast Shelf Sci. 162, 53–68.
Huijts, K.M.H., Schuttelaars, B.H.M., De Swart, H.E., Friedrichs, C.T., 2009. Analytical study of the transverse distribution of along-channel and transverse residual flows in tidal estuaries. Cont. Shelf Res. 29, 89–100.
Jiang, L., Xia, M., 2016. Dynamics of the Chesapeake Bay outflow plume: realistic plume simulation and its seasonal and interannual variability. J. Geophys. Res. Oceans 121, 1424–1445.
Jolliff, J.K., Kindle, J.C., Shulman, I., Penta, B., Friedrichs, M.A.M., Helber, R., Arnone, R.A., 2009. Summary diagrams for coupled hydrodynamic-ecosystem model skill assessment. J. Mar. Syst. 76, 64–82.
Kuijper, K., Van Rijn, L.C., 2011. Analytical and numerical analysis of tides and salinities in estuaries; part II: salinity distributions in prismatic and convergent tidal channels. Ocean Dynam. 61, 1743–1765.
Lacy, J.R., Monismith, S.G., 2001. Secondary currents in a curved, stratified, estuarine channel. J. Geophys. Res. 106, 31283–31302.
Lerczak, J.A., Geyer, W.R., Ralston, D.K., 2008. The temporal response of the length of a partially-stratified estuary to changes in river flow and tidal amplitude. J. Phys. Oceanogr. 39, 915–933.
Lips, U., Laanemets, J., Lips, I., Liblik, T., Suhhova, I., Suursaar, Ü., 2017. Wind-driven residual circulation and related oxygen and nutrient dynamics in the Gulf of Finland (Baltic Sea) in winter. Estuar. Coast Shelf Sci. 195, 4–15.
Liu, B., Peng, S., Liao, Y., Wang, H., 2019. The characteristics and causes of increasingly severe saltwater intrusion in Pearl River Estuary. Estuar. Coast Shelf Sci. 220, 54–63.
MacCready, P.M., Hetland, R.D., Geyer, W.R., 2002. Long-term isohaline salt balance in an estuary. Cont. Shelf Res. 22, 15912–16001.
Mellor, G.L., Yamada, T., 1982. Development of a turbulence closure model for geophysical fluid problems. Rev. Geophys. Space Phys. 20, 851–875.
Montagna, P., Palmer, P., Pollack, J., 2013. Hydrological Changes and Estuarine Dynamics, vol. 8. Springer briefs in Environmental Science, pp. 94. https://doi.org/10.1007/978-1-4614-5833-3.
Monismith, S.G., Kimmerer, W., Stacey, M.T., Burau, J.R., 2002. Structure and flow-induced variability of the subtidal salinity field in Northern San Francisco Bay. J. Phys. Oceanogr. 32, 3003–3019.
Nepf, H.M., Geyer, W.R., 1996. Intratidal variations in stratification and mixing in the Hudson Estuary. J. Geophys. Res. 101, 12079–12086.
Nunes, R.A., Simpson, J.H., 1985. Axial convergence in a well-mixed estuary. Estuar. Coast Shelf Sci. 20, 637–649.
Pasternack, G.B., Hinnov, L.A., 2003. Hydrometeorological controls on water level in a vegetated Chesapeake Bay tidal freshwater delta. Estuar. Coast Shelf Sci. 58, 367–387.
Perales-Valdivia, H., Sanay-González, R., Valle-Levinson, A., 2018. Effects of tides, wind and river discharge on the salt intrusion in a microtidal tropical estuary. Reg. Stud. Mar. Sci. 24, 400–410.
Pinho, J.L.S., Vieira, J.M.P., 2007. Mathematical Modelling of Salt Water Intrusion in a Northern Portuguese Estuary, vol. 310. IAHS-AISH Publication, pp. 277–287.
Pollack, M.J., 1960. Wind set-up and shear-stress coefficient in Chesapeake Bay. J. Geophys. Res. 65, 3383–3389.
Prandle, D., 2004. Saline intrusion in partially mixed estuaries. Estuar. Coast Shelf Sci. 59, 385–397.
Price, J.F., Sundermeyer, M.A., 1999. Stratified ekman layers. J. Geophys. Res. 104, 20467–20494.
Price, F.A., Weller, R.A., Schudlic, R.R., 1987. Wind-driven ocean currents and Ekman transport. Science 238, 1534–1538.
Pritchard, D.W., 1952. Salinity distribution and circulation in the Chesapeake bay esturarine system. J. Mar. Res. 11, 106–123.
Pritchard, D.W., 1954. A study of the salt balance of a coastal plain estuary. J. Mar. Res. 13, 133–144.
Pritchard, D.W., 1956. The dynamic structure of a coastal plain estuary. J. Mar. Res. 15, 33–42.
Ralston, D.K., Geyer, W.R., Lerczak, J.A., 2008. Subtidal salinity and velocity in the Hudson River estuary: observations and modeling. J. Phys. Oceanogr. 38, 753–770.
Smagorinsky, J., 1963. General circulation experiments with the primitive equations, I. The basic experiment. Mon. Weather Rev. 91, 99–164.
Savenije, H.H.G., 1993. Composition and driving mechanisms of longitudinal tidal average salinity dispersion in estuaries. J. Hydrol. 144, 129–141.
Scully, M.E., Friedrichs, C.T., 2007. The importance of tidal and lateral asymmetries in stratification to residual circulation in partially-mixed estuaries. J. Phys. Oceanogr. 37, 1496–S1511.
Simpson, J.H., Brown, J., Matthews, J.G., Allen, G., 1990. Tidal straining, density currents, and stirring in the control of estuarine stratification. Estuaries 13, 125–132.
Simpson, J.H., Williams, E., Brasseur, L.H., Brubaker, J.M., 2005. The impact of tidal straining on the cycle of turbulence in a partially stratified estuary. Cont. Shelf Res. 25, 51–64.
Snedden, G.A., Xu, Y.J., 2016. Drivers of barotropic and baroclinic exchange through an estuarine navigation channel in the Mississippi River Delta Plain. Water 8, 184. https://doi.org/10.3390/w8050184.
Taylor, K.E., 2001. Summarizing multiple aspects of model performance in a single diagram. J. Geophys. Res. 106, 7183–7192.
Tian, R.C., Chen, C., 2006. Influence of model geometrical fitting and turbulence parameterization on phytoplankton simulation in the Gulf of Maine. Deep-Sea Res. II 53, 2808–2832.
Tian, R., Chen, C., Qi, J., Ji, R., Beardsley, R.C., Davis, C., 2014. Model study of nutrient and phytoplankton dynamics in the Gulf of Maine: patterns and drivers for seasonal and interannual variability. ICES (Int. Counc. Explor. Sea) J. Mar. Sci. https://doi.org/10.1093/icesjms/fsu090.
Wang, D.P., 1979a. Wind-driven circulation in Chesapeake bay, winter 1975. J. Phys. Oceanogr. 9, 564–572.
Wang, D.P., 1979b. Subtidal sea level variations in the Chesapeake Bay and relations to atmospheric forcing. J. Phys. Oceanogr. 9, 413–421.
Wang, D.P., Elliott, A.J., 1978. Non-tidal variability in the Chesapeake bay and Potomac River: evidence for non-local forcing. J. Phys. Oceanogr. 8, 225–232.
Wells, M., Cossu, R., 2013. The possible role of Coriolis forces in structuring large-scale sinuous patterns of submarine channel–levee systems. Phil. Trans. R. Soc. A 371, 20120366. https://doi.org/10.1098/rsta.2012.0366.
Xia, N., Jiang, L., 2016. Application of an unstructured grid-based water quality model to Chesapeake Bay and its adjacent coastal ocean. J. Mar. Sci. Eng. 4. https://doi.org/10.3390/jmse4030052.
Xu, J.T., Long, W., Wiggert, J.D., Lanerolle, L.W.J., Brown, C.W., Murtugudde, R., Hood, R.R., 2012. Climate forcing and salinity variability in Chesapeake Bay, USA. Estuar. Coasts 35, 237–261.
Yoon, B.I., Woo, S.B., 2013. Correlation between freshwater discharge and salinity intrusion in Han River Estuary, South Korea. J. Coastal Res. Special Issue 65, 1247–1252.
Zhang, X.F., Deng, J.Q., 2010. Affecting factors of salinity intrusion in Pearl River Estuary and sustainable utilization of water resources in Pearl River Delta. In: Fukushi, K. (Ed.), Sustainability in Food and Water: an Asian Perspective. Springer Science, pp. 11–17.